

Schedule On the Fly: Diffusion Time Prediction for Faster and Better Image Generation

Zilyu Ye^{1,2,†} Zhiyang Chen^{1,4,*} Tiancheng Li^{1,2} Zemin Huang¹ Weijian Luo^{1,3} Guo-Jun Qi^{1,4,*}

¹MAPLE Lab, Westlake University

²South China University of Technology, ³Peking University

⁴Institute of Advanced Technology, Westlake Institute for Advanced Study

zilyuye@foxmail.com, {chenzhiyang, litiancheng, huangzemin}@westlake.edu.cn

luoweijian@stu.pku.edu.cn, guojunq@gmail.com

<https://github.com/maple-research-lab/TPDM>

Abstract

*Diffusion and flow matching models have achieved remarkable success in text-to-image generation. However, these models typically rely on the predetermined denoising schedules for all prompts. The multi-step reverse diffusion process can be regarded as a kind of chain-of-thought for generating high-quality images step by step. Therefore, diffusion models should reason for each instance to adaptively determine the optimal noise schedule, achieving high generation quality with sampling efficiency. In this paper, we introduce the Time Prediction Diffusion Model (TPDM) for this. TPDM employs a plug-and-play Time Prediction Module (TPM) that predicts the next noise level based on current latent features at each denoising step. We train the TPM using reinforcement learning to maximize a reward that encourages high final image quality while penalizing excessive denoising steps. With such an adaptive scheduler, TPDM not only generates high-quality images that are aligned closely with human preferences but also adjusts diffusion time and the number of denoising steps on the fly, enhancing both performance and efficiency. With **Stable Diffusion 3 Medium** architecture, TPDM achieves an aesthetic score of **5.44** and a human preference score (HPS) of **29.59**, while using around 50% fewer denoising steps to achieve better performance.*

1. Introduction

In recent years, deep generative models, including diffusion models [13, 50, 52] have achieved extraordinary per-

formance across a variety of tasks, including image synthesis [18, 19, 43, 44, 47], video generation [4, 14, 64], and others [21, 36, 40, 49]. As a multi-step denoising framework, diffusion models progressively refine random noise into coherent data through iterative sampling, which underlies their impressive capabilities in generating high-quality, diverse outputs.

Inference with a diffusion model involves selecting a noise scheduler, e.g. how the noise level changes step by step when denoising from Gaussian noise. This naturally forms a kind of chain-of-thought [59], as it determines how the model gradually generates a real image. Many works reveal that different noise schedules could greatly affect the model performance [19]. The leading flow-matching models, Stable Diffusion 3 [10] and FLUX [22], provide recommended noise schedulers according to the targets' resolution. Sabour [46] and Xia [61] explore ways to fine-tune the schedule for a model, improving either its efficiency or overall performance. In addition, some one-step generators [16, 33–35] also achieve impressive performance. Despite the excellent performance they achieve, most of these works hold the assumption that there exists a universally applicable schedule that is optimal for all prompts and images, which is doubtful.

Let us see some examples in Fig. 4. The rightmost images contain more complex visual structures generated from longer prompts. These examples make it necessary for the diffusion model to engage a longer chain of sampling steps to generate richer contents. In contrast, the images on the left have simpler structures (e.g., a single object and uniform background) that can be generated with a shorter chain of fewer steps. Moreover, as discussed later, the noise level set by diffusion time t for each step matters a lot in properly determining how a sample should be denoised at various steps to eventually generate a high quality image. Thus, we

The project was supported by MAPLE Lab at Westlake University.

† The work was done during an internship at MAPLE lab.

* Corresponding author. G.-J. Qi conceived and formulated the idea.

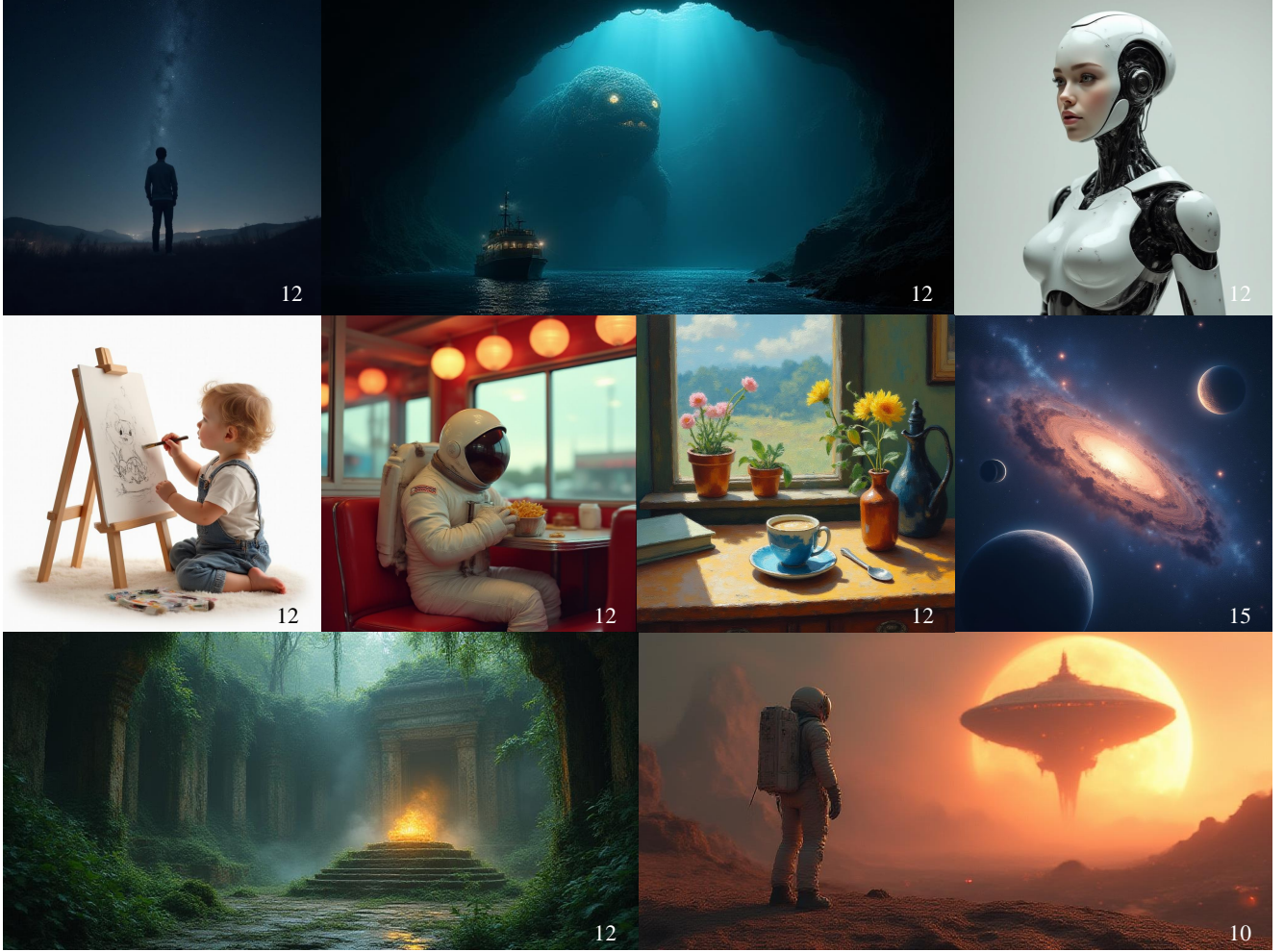


Figure 1. Samples generated by TPDM-FLUX.1-dev showcase stunning visual effects while adaptively adjusting inference steps based on the target output. The number in the lower right corner of each image indicates the inference steps used.

ask: *Is it possible to adaptively determine both the number of denoising steps and the noise level of each step for each chain of reverse diffusion steps leading to its generated image?*

In this paper, we propose Time Prediction Diffusion Models (TPDMs) that can adaptively adjust the noise level at each step as well as the total number of steps during inference. This is achieved by a plug-and-play Time Prediction Module (TPM) that can predict the next diffusion time conditioned on the latent features at the current step. By regarding the reverse diffusion process as a chain of multiple decisions on the diffusion time at each step, we implement reinforcement learning to maximize the reward computed by a reward model aligned with human preference [63]. The reward does not only reflect the quality of the generated image, but is also discounted by the number of steps used in the generation process. Thus, TPDM is directly optimized to generate high-quality images with reduced de-

noising steps. Moreover, TPM can be easily integrated into any diffusion models with marginal additional computation, allowing them to dynamically adjust the noise schedule for better performance and efficiency.

We implement TPDM on several state-of-the-art models, including Stable Diffusion 3 and Flux. With adaptive noise schedulers, TPDM can generate images with 50% fewer steps on average, while keeping the quality on par or slightly better (**0.322 CLIP-T, 5.445 Aesthetic Score, 22.33 Pick Score, 29.59 HPS v2.1**) than Stable Diffusion 3. We visualize some generated images in Fig. 1 as well as the number of steps used. These results demonstrate that TPDM has the potential to either pursue high-quality image generation or improve model efficiency.

Our contributions are summarized below:

- We introduce the Time Prediction Diffusion Model (TPDM). It can predict next diffusion time at each denoising step, determining the optimal noise schedule for

each inference instance.

- We train TPDM with reinforcement learning and maximize a reward with regard to both the quality of the generated image and the number of steps, directly optimizing the final performance and efficiency.
- TPDM demonstrates improved performance across multiple evaluation benchmarks, achieving better results with fewer inference steps.

2. Related Works

2.1. Diffusion Models

Diffusion Probability Models (DPMs) [13, 50] recover the original data from pure Gaussian noise by learning the data distribution across varying noise levels. With their strong adaptability to complex data distributions, diffusion models have achieved remarkable performance in diverse fields such as images [15, 20, 39, 40, 42], videos [4, 14, 28, 64], and others [9, 27, 57, 65, 66], significantly advancing the capabilities of Artificial Intelligence Generated Content.

2.2. Noise Schedule

In order to generate an image, the model must determine the diffusion time for each step. This can be achieved using either discrete-time schedulers [13, 51] or continuous-time schedulers [25, 29] depending on the model. Typically, the diffusion time reflects the noise level at each step, and most existing approaches rely on pre-determined schedulers. Currently, the leading flow-matching models, Stable Diffusion 3[10] and FLUX[22], provide recommended schedulers that adjust noise levels only based on the target resolution.

Some methods optimize the scheduler to speed up sampling or improve image quality. Xia et al. [61] predict a new diffusion time for each step to find a more accurate integration direction, Sabour et al. [46] use stochastic calculus to find the optimal sampling plan for different schedulers and different models. Wang et al. [56] leverage reinforcement learning to automatically search for an optimal sampling scheduler. Also, adjusting the scheduler is also effective in other areas such as molecular generation [17]. Some one-step generators[16, 34, 35] with diffusion distillation [31] also achieve impressive performance.

All of the above noise schedulers not only have high thresholds that require users to adjust some hyper-parameters, but also use the same denoising schedule for all prompts and images. On the contrary, TPDM can adaptively adjust the noise schedule during inference and select the optimal sampling plan with suitable sampling steps for each generation, enhancing image quality and model efficiency. We will introduce the detailed definitions and practical algorithms of TPDM in Sec. 3.

2.3. Reinforcement Learning and Learning from Human Feedback

Reinforcement Learning from Human Feedback (RLHF) has recently gained significant attention in the field of large language models (LLMs) [1, 48, 53] and is gradually expanding into other domains. Advances in diffusion models have increasingly incorporated reward models to enhance alignment with human preferences [23, 60, 63]. By treating latents as actions, diffusion models can be optimized with policy gradient (DDPO [3], DPOK[11]), actor-critic framework (DACER [58]), direct preference optimization (Diffusion-DPO [55]) and other reinforcement algorithms. Some recent works have also studied the RLHF for few-step generative models [32, 37]. Since these approaches rely on the Gaussian reverse processes of the diffusion SDE sampler, however, they are challenging to apply in flow-matching models. On the contrary, in this paper we treat the diffusion time as the action instead of latents. Our goal is to adjust the schedule to achieve better quality with fewer steps, offering a more general and flexible solution.

3. The Proposed Approach

In this section, we first briefly review the fundamental principles of diffusion models, followed by an introduction to the Time Prediction Diffusion Model (TPDM). Finally, we detail the TPDM’s training algorithm.

3.1. Preliminary

Diffusion models learn to generate images with a reverse process that gradually removes noise from a sample. The leading paradigm is flow matching [10, 25]. Thus, we introduce how flow-matching models work, and the detailed structure inside current state-of-the-art models here.

We consider a generative model that establishes a mapping between samples x_1 drawn from a noise distribution p_1 and samples x_0 from a data distribution p_0 . The Flow Matching objective aims to directly regress a vector field v_t , which generates a probability flow, enabling the transition from p_1 to p_0 .

$$\mathcal{L}_{FM}(\theta) = \mathbb{E}_{t, p_t(x)} \|v_\theta(x_t, t) - u(x_t, t)\|^2 \quad (1)$$

The flow-matching model with parameters θ aims to predict the noise prediction function $v_\theta(x_t, t)$, which approximates the true velocity field $u(x_t, t)$ that guides the diffusion process from the noise distribution to the clean distribution of generated samples. Thus, we can get the diffusion ODE:

$$\frac{dx_t}{dt} = v_\theta(x_t, t) \quad (2)$$

During inference, suppose we generate an image with N steps, each step has a time t_n corresponding to its noise

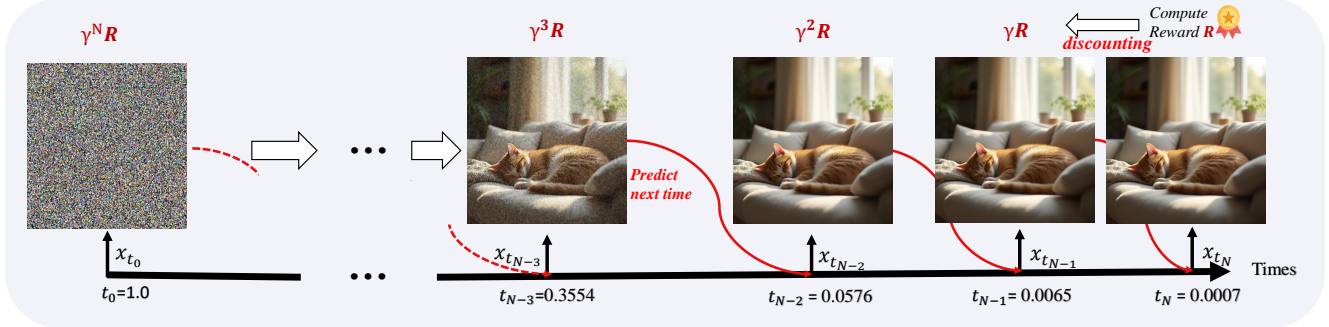


Figure 2. The Inference Process of TPDMs: The horizontal axis represents diffusion time, ranging from 1 to 0. The image starts from random noise x_{t_0} and is progressively denoised until a clean image x_{t_N} . Meanwhile, the reward is calculated for the final image and discounted by γ to influence previous steps.

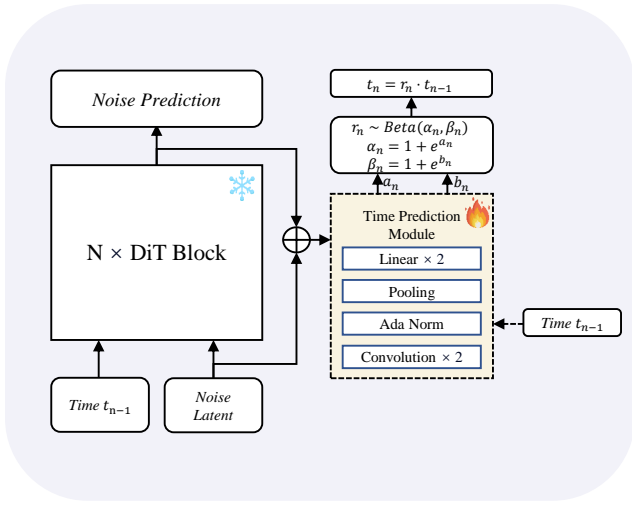


Figure 3. The architecture of TPDM involves a frozen Diffusion Models, and a plug-and-play Time Prediction Module.

level. Then, the n -th generation step can be formulated as:

$$x_{t_n} = x_{t_{n-1}} + (t_n - t_{n-1}) \cdot v_\theta(x_{t_{n-1}}, t_{n-1}) \quad (3)$$

In other words, before the clean image x_{t_N} is finally generated, the model forms a chain of $\{x_{t_n}\}_{n=1}^{N-1}$ as intermediate results. Usually, in a typical flow matching algorithm, there is a pre-determined schedule for each t_n , and the proposed TPDM will dynamically decide it for individual samples.

Currently, many state-of-the-art diffusion models are built upon the DiT architecture [8, 10, 22]. They employ multiple layers of transformers to condition the network on both the diffusion time and the text prompts during denoising steps. In this paper, we will build our TPDM on DiT for the sake of a fair comparison.

3.2. Time Prediction Diffusion Model (TPDM)

To enable the model to adjust the noise schedule on the fly, the TPDM predicts the next diffusion time at each denoising step, as shown in Fig. 2. This can be done by adding a

lightweight Time Prediction Module (TPM) to the diffusion model as shown in Fig. 3. This module concatenates the latent features before and after the DiT blocks as inputs, so that both the original noisy inputs and the denoised results at this step are taken into consideration. Then, after several convolution layers, TPM pools the latent features into a single feature vector for prediction. Moreover, we also use an adaptive normalization layer [41] in TPM so that the model is aware of the current diffusion time.

Diffusion time sets the noise level, which should monotonically decrease throughout the denoising process. To prevent backward progression, at each step, TPM predicts decay rate r instead, which quantifies how much diffusion time t decreases between adjacent steps. Since the reinforcement learning-based training algorithm in Sec. 3.3 requires a probability of the predicted time, the final stage of TPM employs two linear layers to process the pooled features and predict the parameters of distribution of r rather than predicting a deterministic value.

Suppose that we are at the n -th denoising step. The distribution of the decay rate r_n is modeled as a Beta distribution over $(0, 1)$ with two parameters α_n and β_n predicted by TPDM. We note that ensuring $\alpha_n > 1$ and $\beta_n > 1$ results in a unimodal distribution, which is desired as it avoids TPDM from sampling a potentially vague decay rate from a multi-mode beta distribution. To enforce this constraint, we reparameterize the model such that TPDM predicts two real-valued parameters, a_n and b_n , from which α_n and β_n are determined using Eq. 4. Consequently, the decay rate r_n and the next diffusion time t_n can be sampled as in Eq. 5 and Eq. 6.

$$\alpha_n = 1 + e^{a_n}, \quad \beta_n = 1 + e^{b_n}, \quad (4)$$

$$r_n \sim \text{Beta}(\alpha_n, \beta_n) \quad (5)$$

$$t_n = r_n \cdot t_{n-1} \quad (6)$$

During training, we freeze the original diffusion model and only update the newly introduced TPM. Thus, the

model learns to predict the next diffusion time while preserving the original capacity for image generation.

3.3. Training Algorithms

To train TPM, we need to roll out at least two denoising steps: predicting the next diffusion time with the first step, and denoising with it at the next step. A naive method provides a noised image as input to the first step and trains the model with the reconstruction loss calculated at the second step. The gradients would backpropagate through the predicted t_n to update TPM in the first step. However, we found that the trained model tends to complete the denoising process in very few steps during inference, leading to poor image quality. We hypothesize that by supervising the loss calculated after two steps, the model learns to generate a fully denoised image after two steps, and stop intermediate to minimize the loss function. However, what matters is the final image generated after the whole diffusion reverse process, which is ignored in this method.

After summarizing the above failure, we optimize TPM to maximize the image quality generated after the whole denoising process to achieve precise time prediction. The quality is measured by an image reward model [63]. Considering the computational graph of whole inference is too deep for gradients to backpropagate, so we train the model with Proximal Policy Optimization (PPO) [48], whose loss function is formulated as

$$\mathcal{L}(\theta) = - \left[\frac{\pi_\theta(y|s)}{\pi_{\text{old}}(y|s)} \hat{A}(s, y) - \lambda \text{KL}[\pi_{\text{ref}}(\cdot|s), \pi_\theta(\cdot|s)] \right] \quad (7)$$

Under our task, $s = (c, \epsilon)$ denotes initial states including the input prompt c and gaussian noise $\epsilon \sim \mathcal{N}(0, 1)$; π_θ denotes the policy network, e.g. our TPDM model. π_{old} denotes the old policy for sampling trajectories; π_{ref} denotes a reference policy for regularization; y denotes the action our policy takes, i.e., the scheduled time; and $\hat{A}(s, y)$ denotes the advantage the action y has given the state s . We will specify them in the following.

Treat the whole schedule as an action Usually, when the model makes a sequence of predictions, PPO regards every single prediction as an action and optimizes with them as a batch. Recently, RLOO [1] claims that when the reward only appears at the end of the sequence and the state transition is fully deterministic given a sequence element, we can regard the whole sequence as an action with no harm to the performance. Thus for simplicity, the *entire generation*, including all predicted time in the schedule, is considered as a single action to optimize.

Thus, when computing expectation in Eq. 7, we consider the whole trajectory as a training sample in optimization. However, TPDM only outputs the distribution of each single time prediction, which we denote by $\pi_\theta^{(n)}$ for the n -th step.

By the chain rule, the probability of the entire generation can be calculated as the product of each prediction:

$$\pi_\theta(t_1, \dots, t_N|s) = \prod_{n=1}^N \pi_\theta^{(n)}(t_n|s, t_1, \dots, t_{n-1}), \quad (8)$$

where N denotes the total number of the generation steps. In our model, each factor $\pi_\theta^{(n)}$ is computed based on the TPM's output beta distribution at the corresponding step.

Image reward discounted by the number of steps

When generating samples for policy gradient training, we obtain trajectories by generating images from Gaussian noise with the current TPDM policy. Since there exists no ground truth for these generated images, we choose ImageReward [63] to assign a reward score based solely on the final image in the last denoising step. We aim to enhance final image quality without endlessly increasing denoising steps, so we apply a discount factor $\gamma < 1$ (a hyper-parameter) to discount reward to intermediate diffusion steps and calculate the average over the total number of denoising steps N . The final reward for this trajectory is shown in Eq. 9 below

$$R(s, y) = \frac{1}{N} \sum_{n=1}^N \gamma^{N-n} \text{IR}(y, s) \quad (9)$$

where $\text{IR}(y, s)$ denotes the reward of the image generated according to the initial state s and the predicted action y . We refer readers to RLOO [1] on how to compute the advantage $\hat{A}(s, y)$ directly from a batch of $R(s, y)$ without a value model for optimization.

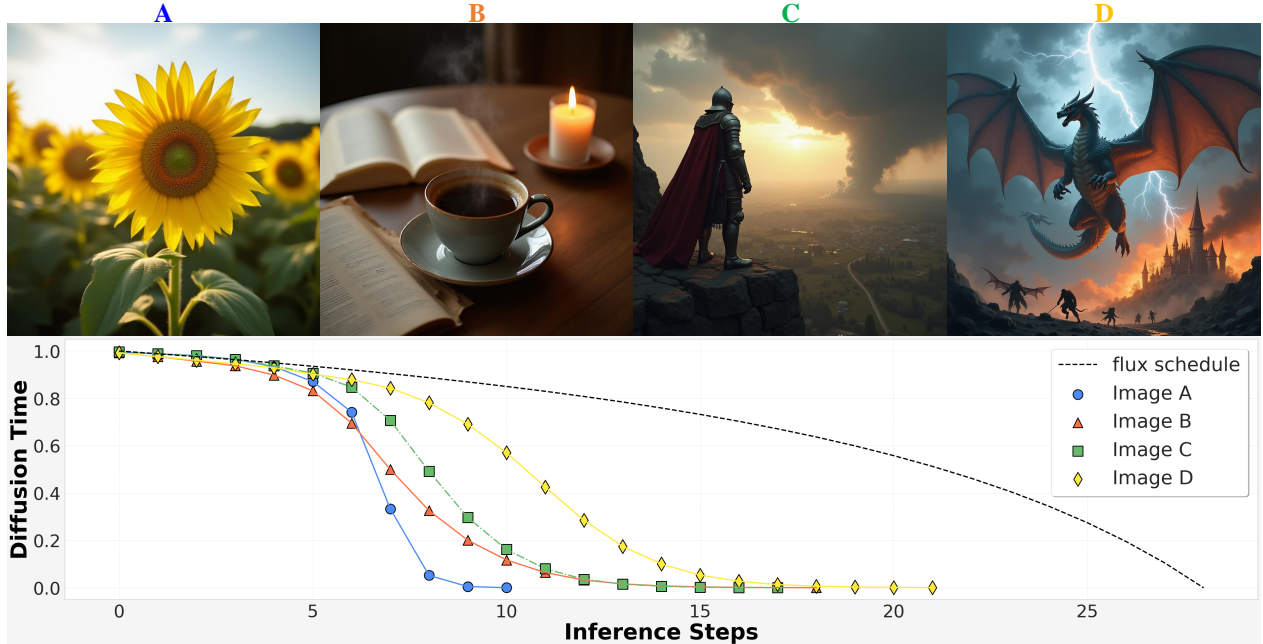
This reward function would encourage TPDM to generate images with higher quality and more efficiently. By adjusting γ , we can control how fast the reward calculated at the final step decays when propagating to previous steps. If a smaller γ is set, the reward will decay faster as the number of steps increases. Thus, the model learns to allocate fewer steps in general. We will elaborate more in Sec. 4.2.

4. Experiments

4.1. Implementation details

Dataset We collect text prompts to train our model. These prompts are either from COCO 2017[24] train set or by captioning images in Laion-Art [54] and COYO-700M [5] datasets with Florence-2 [62] and Llava-Next [26]. We will elaborate on this in Appendix A.

Training Configurations We utilize the AdamW optimizer with beta coefficients of $(0.9, 0.99)$, a constant learning rate of 1×10^{-5} , and a maximum gradient norm of 1.0. Our TPM module typically requires only 200 training steps. In each step, we sample a batch size of 256 trajectories, and update the model parameter 4 times with them.

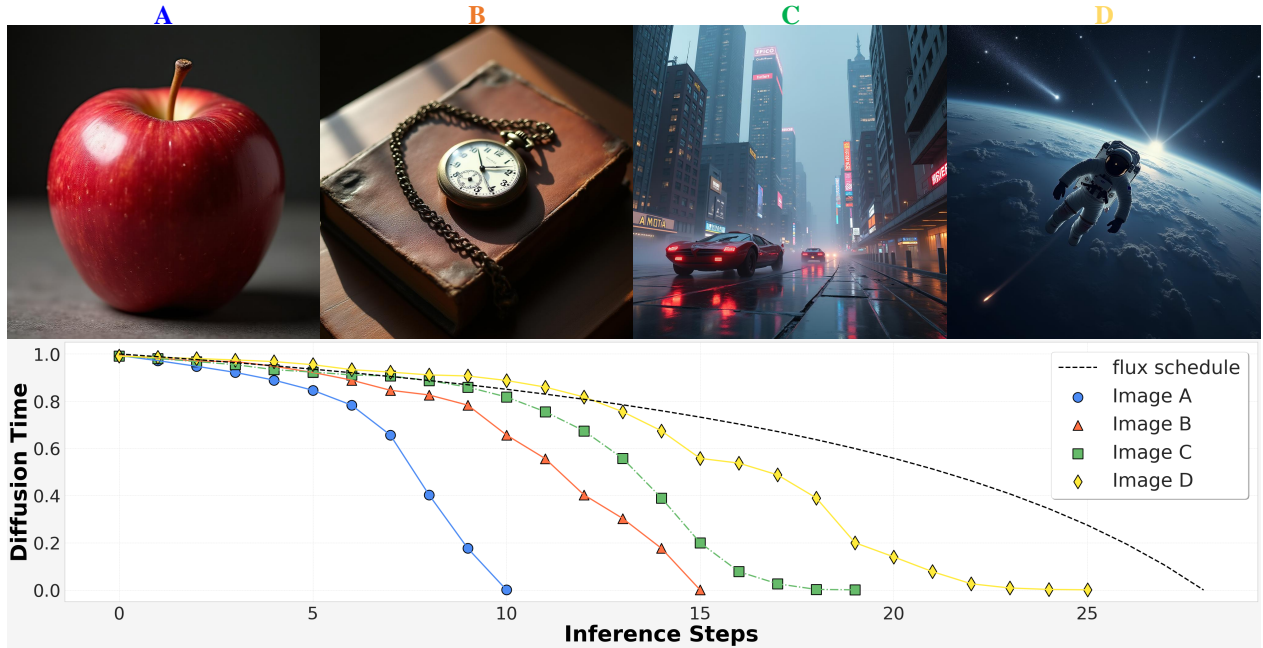


A: A bright yellow sunflower in a field on a sunny day.

B: A steaming cup of coffee on a wooden table, surrounded by open books and a flickering candle.

C: A medieval knight in shining armor standing on a cliff, overlooking a vast battlefield at dawn, with a storm approaching in the distance.

D: A majestic dragon soaring through a stormy sky, with lightning flashing around it, and a burning castle below, as mythical creatures run through the smoke and chaos.



A: A single red apple.

B: A vintage pocket watch lying on an old leather-bound book, with soft sunlight casting gentle shadows.

C: A futuristic cityscape at dusk, with sleek flying cars, towering skyscrapers, and neon signs glowing in the mist.

D: An astronaut floating in space, with Earth visible in the background, surrounded by swirling galaxies and distant stars, while a comet streaks across the sky.

Figure 4. From left to right, the images generated by TPDM-FLUX1.0-dev progress from simple to complex. Our Time Prediction Module adaptively adjusts the generation schedule to suit the complexity of each generation target.

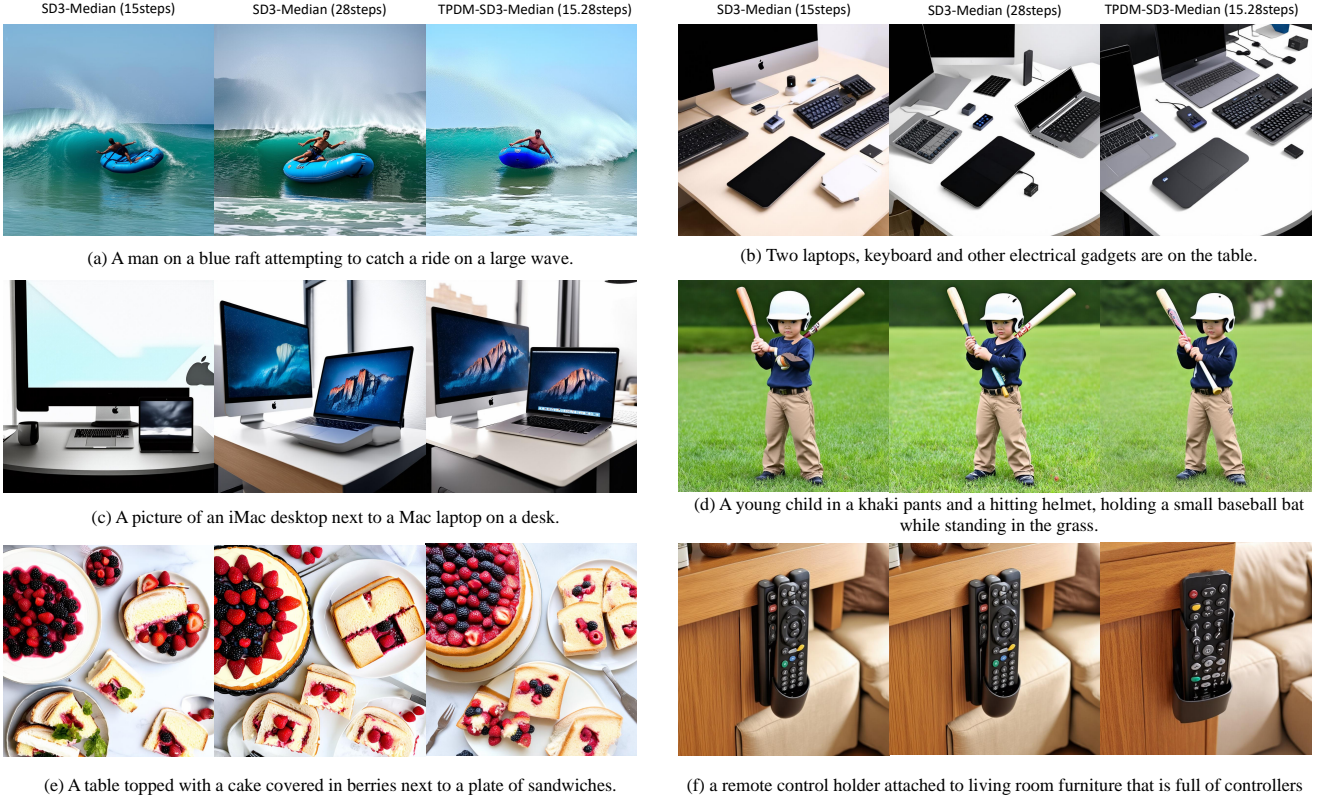


Figure 5. Our TPDM-SD3-Medium, when compared to the SD3-Medium with the recommended and equivalent number of steps, demonstrates superior detail processing ability and generation accuracy.

Evaluation Metrics We use FID, CLIP-T, Aesthetic v2, and Pick Score as evaluation metrics by testing with 5,000 prompts from COCO 2017 validation set. For HPS v2.1, we use the 3,200 prompts provided by the benchmark [60].

4.2. Main Results

Adaptive Schedule for Different Images In Fig. 4, we present images generated with different prompts and their corresponding schedules predicted by TPDM. When prompting TPDM with shorter and simpler prompts, it requires fewer objects and details to appear in the generated image. Thus the diffusion time decreases faster and reaches 0 in relatively fewer steps. On the contrary, when more complex prompts are provided, the model needs to reason with more intermediate steps, so that it can generate more delicate details at early and middle stages. Therefore, the diffusion time decreases more slowly. In this case, TPDM requires more denoising steps in the generation process. In the Appendix C, we provide more examples of predicted schedules for analysis.

Adjusting γ for Different Number of Steps γ in Eq. 9 controls how fast the reward decays when propagating from the final step to intermediate steps, as shown in Fig. 2, thereby affecting the average number of denoising steps of

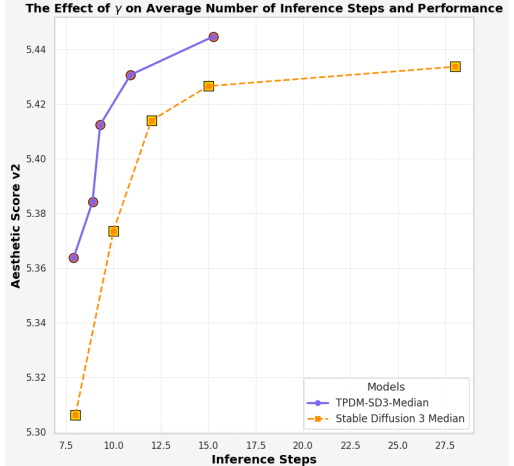


Figure 6. The effect of γ on the average number of inference steps.

our converged TPDM.

As shown in Fig. 6, as we decrease γ from 0.97 to 0.85, TPDM tends to decrease the diffusion time more rapidly, leading to fewer denoising steps, from 15.0 to 7.5. Additionally, when compared to the baseline (yellow line), TPDM (purple line) consistently achieves a significantly higher aesthetic score with the same number of inference

Models	Inference Steps	FID	CLIP-T	Aesthetic v2	Pick Score	HPSv2.1
SD3-Medium [10]	28	<u>25.00</u>	0.322	<u>5.433</u>	22.12	<u>29.12</u>
	15	24.72	0.321	5.426	<u>22.30</u>	28.52
	15.28	25.26	0.322	5.445	22.33	29.59
TPDM-SD3-Medium	28	23.29	0.318	5.487	22.81	30.85
	15	<u>23.35</u>	0.323	5.475	22.62	30.02
	15.22	24.48	<u>0.322</u>	5.525	22.81	30.64
FLUX.1-dev [22]	28	<u>29.09</u>	0.308	<u>5.622</u>	23.03	31.94
	15	29.10	0.306	5.613	22.86	<u>31.14</u>
	13.57	28.98	0.314	5.685	<u>22.94</u>	30.77

Table 1. Evaluation of models across various benchmarks. The best result is highlighted in bold, and the second best result is underlined

steps.

Visual Comparison Fig.5 provides some specific images generated by both TPDM and SD3-Medium. In Fig. 5(c), the image generated by TPDM have a more realistic laptop keyboard than SD3-Medium with 15 and 28 steps. As for Fig.5(d), TPDM removes the extra baseball bat, leading to a more natural looking. Generally, TPDM is able to generate more accurate and realistic images.

4.3. Quantitative Results

We apply TPM on several state-of-the-art diffusion models, including SD3-Medium, SD3.5-Large, and Flux 1.0 dev, and demonstrate how TPM could enhance their performance. Other than commonly used metrics like FID, CLIP-T and human preference scores (Aesthetic Score v2, and HPSv2.1), we provide a user study as well.

Quantitative Metrics We compared TPDM and the above-mentioned models in Tab. 1. While maintaining competitive performance, TPDM can generate images in about half of their recommended steps on average.

Among all the metrics, those representing human preference improve the most. For example, by generating with just 15.28 steps on average, TPDM-SD3-Medium gets a 29.59 HPS score, +1.07 higher than Stable Diffusion 3 with similar steps, also +0.47 higher than the original 28-step results. This improvement may be attributed to the reward model, which is well aligned with human preferences. By optimizing image generation based on this alignment, TPDM produces more aesthetically pleasing results. Furthermore, since other scheduler optimization methods mostly conduct experiments on classical diffusion models such as Stable Diffusion 1.5 [45], we conduct an apple-to-apple comparison with them in Appendix B as well.

User Study To better reflect human preference towards these models, we conduct a user study by inviting volunteers to compare images generated from different models.

Specifically, for each prompt, we provide two images generated by SD3-Medium with 15 and 28 steps separately, and an image generated by TPDM-SD3-Medium. We generate 50 groups of images for comparison in total, and in-

Models	Inference Steps	Win Rate
SD3-Medium	28	26.58%
SD3-Medium	15	16.40%
TPDM-SD3-Medium	15.28	47.25%

Table 2. User study based on Stable Diffusion 3 architecture

TPM inputs	Steps	FID	CLIP-T	PickScore	Aes v2
First 2 Layers	16.20	24.81	0.321	22.18	5.400
Last 2 Layers	19.30	23.19	0.322	22.16	5.356
First & Last Layers	15.28	25.26	0.322	22.33	5.445

Table 3. Ablation Study of inputs hidden states

vite 15 volunteers to select the ones they prefer. The result is shown in Tab. 2, indicating that our model can generate images that better align human preferences.

Ablation on the Architecture Tab. 3 indicates that taking features from both the first and last layer as the inputs for TPM performs better than only taking features from either the beginning or last two layers.

5. Conclusions and Limitations

In this paper, we view denoising steps as a kind of chain-of-thought in image generation, and introduce the Time Prediction Diffusion Model (TPDM) by adaptively predicting the next diffusion time to denoise images in the reverse diffusion process. This adjusts the noise schedule per sample, optimizing image generation for each prompt. By aligning the final outputs of the denoising process with human preferences, TPDM can reduce the number of inference steps by almost 50% while still keeping image quality.

Limitations. First, in this paper, we only design a simple architecture for TPM. A more delicate module may yield better performance. Second, we freeze the parameters of the original diffusion model. Updating them iteratively with the training of TPM could lead to improved results, which is left for further exploration.

Acknowledgement. This work was supported by National Natural Science Foundation of China under Grant No. 92467104, and Zhejiang Leading Innovative and Entrepreneur Team Introduction Program (2024R01007).

References

[1] Arash Ahmadian, Chris Cremer, Matthias Gallé, Marzieh Fadaee, Julia Kreutzer, Olivier Pietquin, Ahmet Üstün, and Sara Hooker. Back to Basics: Revisiting REINFORCE Style Optimization for Learning from Human Feedback in LLMs, 2024. 3, 5

[2] Stability AI. Stable diffusion 3.5 large. <https://huggingface.co/stabilityai/stable-diffusion-3.5-large>, 2024. 8

[3] Kevin Black, Michael Janner, Yilun Du, Ilya Kostrikov, and Sergey Levine. Training Diffusion Models with Reinforcement Learning, 2023. 3

[4] Andreas Blattmann, Tim Dockhorn, Sumith Kulal, Daniel Mendelevitch, Maciej Kilian, Dominik Lorenz, Yam Levi, Zion English, Vikram Voleti, Adam Letts, Varun Jampani, and Robin Rombach. Stable video diffusion: Scaling latent video diffusion models to large datasets, 2023. 1, 3

[5] Minwoo Byeon, Beomhee Park, Haecheon Kim, Sungjun Lee, Woonhyuk Baek, and Saehoon Kim. Coyo-700m: Image-text pair dataset. <https://github.com/kakaobrain/coyo-dataset>, 2022. 5

[6] CaptionEmporium. coyo-hd-11m-llavanext. <https://huggingface.co/datasets/CaptionEmporium/coyo-hd-11m-llavanext>, 2024. 1

[7] Defang Chen, Zhenyu Zhou, Can Wang, Chunhua Shen, and Siwei Lyu. On the trajectory regularity of ode-based diffusion sampling, 2024. 2

[8] Junsong Chen, Jincheng Yu, Chongjian Ge, Lewei Yao, Enze Xie, Yue Wu, Zhongdao Wang, James Kwok, Ping Luo, Huchuan Lu, and Zhenguo Li. PixArt-\$\alpha\$: Fast Training of Diffusion Transformer for Photorealistic Text-to-Image Synthesis, 2023. 4

[9] Wei Deng, Weijian Luo, Yixin Tan, Marin Biloš, Yu Chen, Yuriy Nevmyvaka, and Ricky TQ Chen. Variational schrödinger diffusion models. *arXiv preprint arXiv:2405.04795*, 2024. 3

[10] Patrick Esser, Sumith Kulal, Andreas Blattmann, Rahim Entezari, Jonas Müller, Harry Saini, Yam Levi, Dominik Lorenz, Axel Sauer, Frederic Boesel, Dustin Podell, Tim Dockhorn, Zion English, Kyle Lacey, Alex Goodwin, Yannik Marek, and Robin Rombach. Scaling Rectified Flow Transformers for High-Resolution Image Synthesis, 2024. 1, 3, 4, 8

[11] Ying Fan, Olivia Watkins, Yuqing Du, Hao Liu, Moonkyung Ryu, Craig Boutilier, Pieter Abbeel, Mohammad Ghavamzadeh, Kangwook Lee, and Kimin Lee. Dpok: Reinforcement learning for fine-tuning text-to-image diffusion models, 2023. 3

[12] Tinglei Feng, Yingjie Zhai, Jufeng Yang, Jie Liang, Deng-Ping Fan, Jing Zhang, Ling Shao, and Dacheng Tao. Ic9600: A benchmark dataset for automatic image complexity assessment. *IEEE Transactions on Pattern Analysis and Machine Intelligence*, 45(7):8577–8593, 2022. 2

[13] Jonathan Ho, Ajay Jain, and Pieter Abbeel. Denoising diffusion probabilistic models, 2020. 1, 3

[14] Jonathan Ho, Tim Salimans, Alexey Gritsenko, William Chan, Mohammad Norouzi, and David J Fleet. Video diffusion models. *arXiv preprint arXiv:2204.03458*, 2022. 1, 3

[15] Emiel Hoogeboom, Victor Garcia Satorras, Clément Vignac, and Max Welling. Equivariant diffusion for molecule generation in 3d. In *International Conference on Machine Learning*, pages 8867–8887. PMLR, 2022. 3

[16] Zemin Huang, Zhengyang Geng, Weijian Luo, and Guojun Qi. Flow generator matching. *arXiv preprint arXiv:2410.19310*, 2024. 1, 3

[17] Hojung Jung, Youngrok Park, Laura Schmid, Jaehyeong Jo, Dongkyu Lee, Bongsang Kim, Se-Young Yun, and Jinwoo Shin. Conditional synthesis of 3d molecules with time correction sampler, 2024. 3

[18] Tero Karras, Samuli Laine, Miika Aittala, Janne Hellsten, Jaakko Lehtinen, and Timo Aila. Analyzing and improving the image quality of stylegan. In *Proceedings of the IEEE/CVF conference on computer vision and pattern recognition*, pages 8110–8119, 2020. 1

[19] Tero Karras, Miika Aittala, Timo Aila, and Samuli Laine. Elucidating the design space of diffusion-based generative models. In *Proc. NeurIPS*, 2022. 1

[20] Heeseung Kim, Sungwon Kim, and Sungroh Yoon. Guided-tts: A diffusion model for text-to-speech via classifier guidance. In *International Conference on Machine Learning*, pages 11119–11133. PMLR, 2022. 3

[21] Zhifeng Kong, Wei Ping, Jiaji Huang, Kexin Zhao, and Bryan Catanzaro. Diffwave: A versatile diffusion model for audio synthesis. In *International Conference on Learning Representations*, 2020. 1

[22] Black Forest Lab. Announcing Black Forest Labs. <https://blackforestlabs.ai/announcing-black-forest-labs/>, 2024. 1, 3, 4, 8

[23] Youwei Liang, Junfeng He, Gang Li, Peizhao Li, Arseniy Klimovskiy, Nicholas Carolan, Jiao Sun, Jordi Pont-Tuset, Sarah Young, Feng Yang, Junjie Ke, Krishnamurthy Dj Dvijotham, Katie Collins, Yiwen Luo, Yang Li, Kai J. Kohlhoff, Deepak Ramachandran, and Vidhya Navalpakkam. Rich Human Feedback for Text-to-Image Generation, 2024. 3

[24] Tsung-Yi Lin, Michael Maire, Serge Belongie, James Hays, Pietro Perona, Deva Ramanan, Piotr Dollár, and C Lawrence Zitnick. Microsoft coco: Common objects in context. In *European conference on computer vision*, pages 740–755. Springer, 2014. 5, 1

[25] Yaron Lipman, Ricky T. Q. Chen, Heli Ben-Hamu, Maximilian Nickel, and Matt Le. Flow Matching for Generative Modeling, 2023. 3

[26] Haotian Liu, Chunyuan Li, Yuheng Li, Bo Li, Yuanhan Zhang, Sheng Shen, and Yong Jae Lee. Llava-next: Improved reasoning, ocr, and world knowledge, 2024. 5, 1

[27] Jinxiu Liu and Qi Liu. R3cd: Scene graph to image generation with relation-aware compositional contrastive control diffusion. In *Proceedings of the AAAI Conference on Artificial Intelligence*, pages 3657–3665, 2024. 3

[28] Jinxiu Liu, Shaoheng Lin, Yinxiao Li, and Ming-Hsuan Yang. Dynamicscaler: Seamless and scalable video generation for panoramic scenes. *arXiv preprint arXiv:2412.11100*, 2024. 3

[29] Xingchao Liu, Chengyue Gong, and Qiang Liu. Flow straight and fast: Learning to generate and transfer data with rectified flow, 2022. 3

[30] Cheng Lu, Yuhao Zhou, Fan Bao, Jianfei Chen, Chongxuan Li, and Jun Zhu. Dpm-solver++: Fast solver for guided sampling of diffusion probabilistic models, 2023. 2

[31] Weijian Luo. A comprehensive survey on knowledge distillation of diffusion models. *arXiv preprint arXiv:2304.04262*, 2023. 3

[32] Weijian Luo. Diff-instruct++: Training one-step text-to-image generator model to align with human preferences. *arXiv preprint arXiv:2410.18881*, 2024. 3

[33] Weijian Luo, Tianyang Hu, Shifeng Zhang, Jiacheng Sun, Zhenguo Li, and Zhihua Zhang. Diff-instruct: A universal approach for transferring knowledge from pre-trained diffusion models. *ArXiv*, abs/2305.18455, 2023. 1

[34] Weijian Luo, Tianyang Hu, Shifeng Zhang, Jiacheng Sun, Zhenguo Li, and Zhihua Zhang. Diff-instruct: A universal approach for transferring knowledge from pre-trained diffusion models. *Advances in Neural Information Processing Systems*, 36, 2024. 3

[35] Weijian Luo, Zemin Huang, Zhengyang Geng, J Zico Kolter, and Guo-jun Qi. One-step diffusion distillation through score implicit matching. *arXiv preprint arXiv:2410.16794*, 2024. 1, 3

[36] Weijian Luo, Boya Zhang, and Zhihua Zhang. Entropy-based training methods for scalable neural implicit samplers. *Advances in Neural Information Processing Systems*, 36, 2024. 1

[37] Weijian Luo, Colin Zhang, Debing Zhang, and Zhengyang Geng. Diff-instruct*: Towards human-preferred one-step text-to-image generative models. *arXiv preprint arXiv:2410.20898*, 2024. 3

[38] George A Miller. Wordnet: a lexical database for english. *Communications of the ACM*, 38(11):39–41, 1995. 1

[39] Alex Nichol and Prafulla Dhariwal. Improved denoising diffusion probabilistic models. *arXiv preprint arXiv:2102.09672*, 2021. 3

[40] Aaron van den Oord, Sander Dieleman, Heiga Zen, Karen Simonyan, Oriol Vinyals, Alex Graves, Nal Kalchbrenner, Andrew Senior, and Koray Kavukcuoglu. Wavenet: A generative model for raw audio. *arXiv preprint arXiv:1609.03499*, 2016. 1, 3

[41] Ethan Perez, Florian Strub, Harm de Vries, Vincent Dumoulin, and Aaron Courville. Film: Visual reasoning with a general conditioning layer, 2017. 4

[42] Ben Poole, Ajay Jain, Jonathan T Barron, and Ben Mildenhall. Dreamfusion: Text-to-3d using 2d diffusion. *arXiv preprint arXiv:2209.14988*, 2022. 3

[43] Aditya Ramesh, Mikhail Pavlov, Gabriel Goh, Scott Gray, Chelsea Voss, Alec Radford, Mark Chen, and Ilya Sutskever. Zero-shot text-to-image generation. In *International Conference on Machine Learning*, pages 8821–8831. PMLR, 2021. 1

[44] Aditya Ramesh, Prafulla Dhariwal, Alex Nichol, Casey Chu, and Mark Chen. Hierarchical text-conditional image generation with clip latents. *arXiv preprint arXiv:2204.06125*, 2022. 1

[45] Robin Rombach, Andreas Blattmann, Dominik Lorenz, Patrick Esser, and Björn Ommer. High-resolution image synthesis with latent diffusion models, 2022. 8, 1, 2

[46] Amirmojtaba Sabour, Sanja Fidler, and Karsten Kreis. Align Your Steps: Optimizing Sampling Schedules in Diffusion Models, 2024. 1, 3, 2

[47] Chitwan Saharia, William Chan, Saurabh Saxena, Lala Li, Jay Whang, Emily Denton, Seyed Kamyar Seyed Ghasemipour, Burcu Karagol Ayan, S Sara Mahdavi, Rapha Gontijo Lopes, et al. Photorealistic text-to-image diffusion models with deep language understanding. *arXiv preprint arXiv:2205.11487*, 2022. 1

[48] John Schulman, Filip Wolski, Prafulla Dhariwal, Alec Radford, and Oleg Klimov. Proximal Policy Optimization Algorithms, 2017. 3, 5

[49] Shuai Shen, Wenliang Zhao, Zibin Meng, Wanhu Li, Zheng Zhu, Jie Zhou, and Jiwen Lu. Difftalk: Crafting diffusion models for generalized audio-driven portraits animation, 2023. 1

[50] Jascha Sohl-Dickstein, Eric A. Weiss, Niru Maheswaranathan, and Surya Ganguli. Deep unsupervised learning using nonequilibrium thermodynamics, 2015. 1, 3

[51] Jiaming Song, Chenlin Meng, and Stefano Ermon. Denoising diffusion implicit models, 2022. 3

[52] Yang Song, Jascha Sohl-Dickstein, Diederik P. Kingma, Abhishek Kumar, Stefano Ermon, and Ben Poole. Score-based generative modeling through stochastic differential equations, 2021. 1

[53] Nisan Stiennon, Long Ouyang, Jeffrey Wu, Daniel Ziegler, Ryan Lowe, Chelsea Voss, Alec Radford, Dario Amodei, and Paul F Christiano. Learning to summarize with human feedback. In *Advances in Neural Information Processing Systems*, pages 3008–3021. Curran Associates, Inc., 2020. 3

[54] Laion Team. Laion-art. <https://huggingface.co/datasets/laion/laion-art>, 2024. 5, 1

[55] Bram Wallace, Meihua Dang, Rafael Rafailov, Linqi Zhou, Aaron Lou, Senthil Purushwalkam, Stefano Ermon, Caiming Xiong, Shafiq Joty, and Nikhil Naik. Diffusion model alignment using direct preference optimization, 2023. 3

[56] Yunke Wang, Xiyu Wang, Anh-Dung Dinh, Bo Du, and Charles Xu. Learning to schedule in diffusion probabilistic models. In *Proceedings of the 29th ACM SIGKDD Conference on Knowledge Discovery and Data Mining*, page 2478–2488, New York, NY, USA, 2023. Association for Computing Machinery. 3

[57] Yifei Wang, Weimin Bai, Weijian Luo, Wenzheng Chen, and He Sun. Integrating amortized inference with diffusion models for learning clean distribution from corrupted images. *arXiv preprint arXiv:2407.11162*, 2024. 3

[58] Yinuo Wang, Likun Wang, Yuxuan Jiang, Wenjun Zou, Tong Liu, Xujie Song, Wenxuan Wang, Liming Xiao, Jiang Wu, Jingliang Duan, and Shengbo Eben Li. Diffusion actor-critic with entropy regulator, 2024. 3

[59] Jason Wei, Xuezhi Wang, Dale Schuurmans, Maarten Bosma, Fei Xia, Ed Chi, Quoc V Le, Denny Zhou, et al.

Chain-of-thought prompting elicits reasoning in large language models. *Advances in neural information processing systems*, 35:24824–24837, 2022. 1

[60] Xiaoshi Wu, Yiming Hao, Keqiang Sun, Yixiong Chen, Feng Zhu, Rui Zhao, and Hongsheng Li. Human Preference Score v2: A Solid Benchmark for Evaluating Human Preferences of Text-to-Image Synthesis, 2023. 3, 7

[61] Mengfei Xia, Yujun Shen, Changsong Lei, Yu Zhou, Ran Yi, Deli Zhao, Wenping Wang, and Yong-jin Liu. Towards More Accurate Diffusion Model Acceleration with A Timestep Aligner, 2023. 1, 3

[62] Bin Xiao, Haiping Wu, Weijian Xu, Xiyang Dai, Houdong Hu, Yumao Lu, Michael Zeng, Ce Liu, and Lu Yuan. Florence-2: Advancing a unified representation for a variety of vision tasks. *arXiv preprint arXiv:2311.06242*, 2023. 5, 1

[63] Jiazheng Xu, Xiao Liu, Yuchen Wu, Yuxuan Tong, Qinkai Li, Ming Ding, Jie Tang, and Yuxiao Dong. Imagereward: Learning and evaluating human preferences for text-to-image generation, 2023. 2, 3, 5

[64] Zhuoyi Yang, Jiayan Teng, Wendi Zheng, Ming Ding, Shiyu Huang, Jiazheng Xu, Yuanming Yang, Wenyi Hong, Xiaohan Zhang, Guanyu Feng, Da Yin, Xiaotao Gu, Yuxuan Zhang, Weihan Wang, Yean Cheng, Ting Liu, Bin Xu, Yuxiao Dong, and Jie Tang. Cogvideoox: Text-to-video diffusion models with an expert transformer, 2024. 1, 3

[65] Zilyu Ye, Jinxiu Liu, Ruotian Peng, Jinjin Cao, Zhiyang Chen, Yiyang Zhang, Ziwei Xuan, Mingyuan Zhou, Xiaqian Shen, Mohamed Elhoseiny, Qi Liu, and Guo-Jun Qi. Openstory++: A large-scale dataset and benchmark for instance-aware open-domain visual storytelling, 2024. 3

[66] Boya Zhang, Weijian Luo, and Zhihua Zhang. Enhancing adversarial robustness via score-based optimization. *Advances in Neural Information Processing Systems*, 36:51810–51829, 2023. 3

Schedule On the Fly: Diffusion Time Prediction for Faster and Better Image Generation

Supplementary Material

A. Dataset Details

In Section 4, we provide a brief overview of our training dataset. Below, we present a more detailed description of the dataset.

A.1. Dataset Source

We curated training prompts from three high-quality datasets, COCO [24], Laion-art [54] and COYO-11M [6].

For COCO, the original captions in the training split is used. For Laion-art, we caption the images with Florence-2 [62] to obtain the text prompts. For COYO-11M, we retained its original captioning by Llava-next [26]. Fig. 7 illustrates the distribution of prompt length after tokenization.

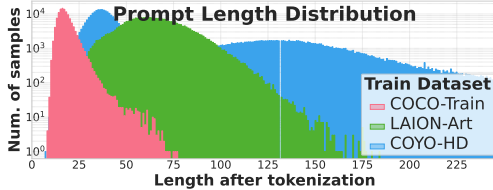


Figure 7. Prompt length distribution.

To ensure diversity during training, we design a filtering pipeline to select a diverse subset of these prompts.

A.2. Filtering Pipeline

Our filtering pipeline, depicted in Figure 8, aims to select diverse and high-quality prompts by analyzing key linguistic features, such as nouns, prepositions, and adjectives. To assess diversity, we utilize *WordNet* [38] to count the number of valid nouns, adjectives, and prepositions in each prompt.

Prompts are ranked based on these counts. Those exhibiting the highest scores are included in the training set. The selection process prioritizes **noun-diversity**, ensuring a balanced representation across categories such as *Person*, *Animal*, *Plant*, *Artifacts (Large/Small Objects)*, and *Natural Views*. Next, prompts with high **preposition-diversity** are selected, emphasizing those that contain spatial and relational terms (e.g., *near*, *on*). Finally, prompts are evaluated for **adjective-diversity**, with particular focus on adjectives describing *color* and *shape*, to enhance descriptive richness.

The process is iterative, selecting the top prompts in order of their noun, adjective, and preposition diversity scores

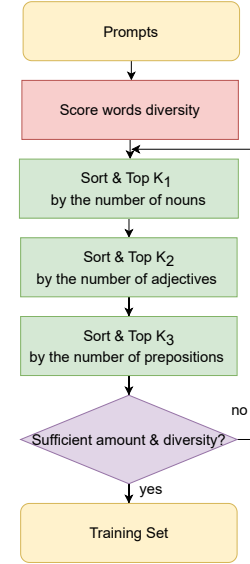


Figure 8. The filtering pipeline used to construct the training set.

until the desired data quantity (51,200 prompts, as specified in Section 4.1) and diversity are achieved. As shown in Figure 9, the diversity of the training set has significantly enhanced after filtering.

B. Application on Denoising Diffusion Probabilistic Models (DDPMs)

Before the widespread use of flow-matching models, diffusion models dominated image generation, such as DDPM [13] and LDM [45]. They demonstrate several differences from flow models during inference. First, they directly predict the noise added to the data at each step, rather than predicting the velocity vector field. Second, both the diffusion time t and the noise level are typically discrete, unlike continuous time in flow-matching models.

In this section, we integrate TPM into Stable Diffusion v1.5 [45], demonstrating that TPM also works with DDPMs. At diffusion time t_{n-1} , to determine the next diffusion time t_n , TPM predicts two real-valued parameters, a_n and b_n . These parameters define α_n and β_n , which shape the Beta distribution of the diffusion time decay rate r_n ,

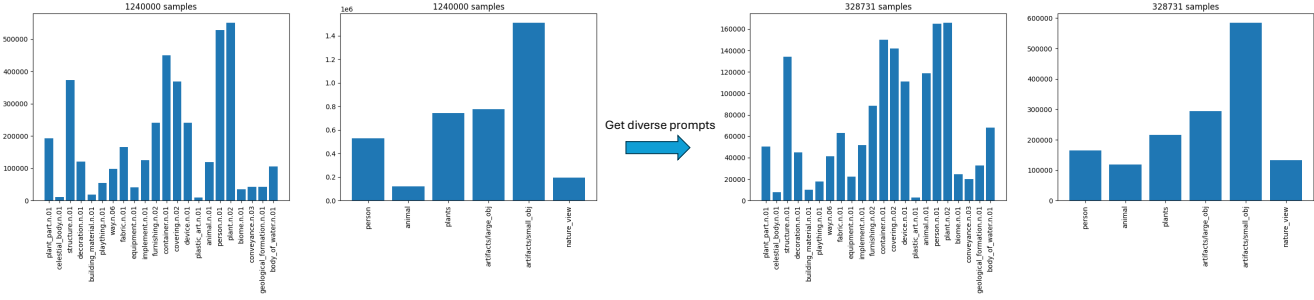


Figure 9. The statistics of prompts from the re-captioned high-resolution Laion-Art dataset, before and after filtering, highlight an improvement in diversity. Our dataset demonstrates greater variety compared to the original.

Method	Inference Steps	FID	CLIP-T	Aesthetic v2	Pick Score	HPSv2.1
DPM-Solver++ [30]	10	21.08	0.314	5.219	21.30	24.00
DPM-Solver++ & AYS [46]	10	18.81	0.313	5.156	21.31	24.40
DPM-Solver++ & GITS [7]	10	18.32	0.313	5.108	21.19	23.72
DPM-Solver++ & TPM	9.89	18.31	0.313	5.118	21.32	24.29

Table 4. Experiments on Stable Diffusion v1.5 [45], and 9.89 is the average number of steps TPM used. The best results are highlighted in bold.

similar to the flow-matching model version of TPDM introduced in 3.2. Then t_n is obtained using Eq. 6 and quantized to the nearest discrete diffusion time to obtain the corresponding noise level.

We compare the performance of TPDM with other scheduler optimization methods applied to diffusion models. The evaluation metrics are calculated using 5,000 prompts from the COCO 2017 validation set, in line with the evaluation protocol as in Table 1. Notably, our findings reveal that TPM can be combined with higher-order solvers, such as DPM-Solver++ [30], resulting in a significant improvement of -2.79 in FID, surpassing the performance of other methods as reported in Tab. 4.

C. Analysis of the Predicted Schedule

Fig. 11 provides more examples to show the noise schedule predicted by TPDM.

We observe that TPDM tends to allocate more inference steps to higher noise levels to generate complex details and layouts. Take Fig. 11(a) for an example where multiple objects of various sizes are generated with a complex visual layout – TPDM allocates 10 out of 17 steps to more noisy diffusion time with $t > 0.8$. This way, TPDM more efficiently spends its inference steps on denoising noisier samples at the earlier stage so that it can add more complex visual layouts and details as early as possible to eventually generate high quality results. It avoids the problem in the benchmark diffusion model that may waste many evenly allocated steps to denoise cleaner images at the later stage. The steep curve in Fig. 11(c) indicates that, for simple gen-

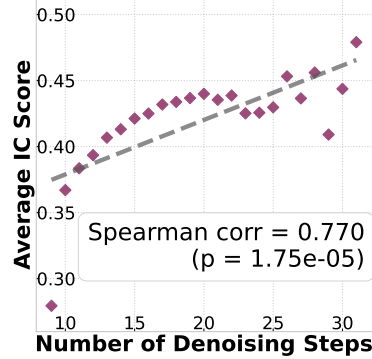


Figure 10. Correlation between the number of steps and image complexity (measured by ICNet [12]).

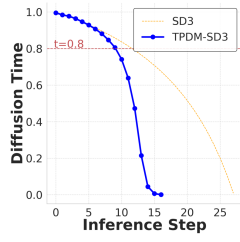
eration, TPDM reduces the diffusion time much faster to almost zero within only 13 steps, instead of evenly allocating 28 steps in the benchmark model. Fig. 11(e) and 11(f) also visualize the results for extremely long prompts. They exhibit a similar trend.

Moreover, Fig. 4 shows that simple prompts lead to faster decrease in diffusion time with fewer steps, while complex ones lead to more steps. We use ICNet [12] to score the image complexity, and calculate the average score of images generated with different number of steps in evaluation set. As shown in Fig. 10, it has a high correlation efficient (0.770), which supports our assumption that complex images are dynamically generated with more steps by TPDM.

Prompt: Seabed wonderland, schools of fish, seashells, multi-sized corals.



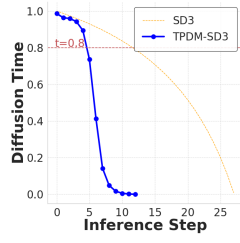
(a)



Prompt: Snowy peak, soaring eagle, icy winds, blue sky.



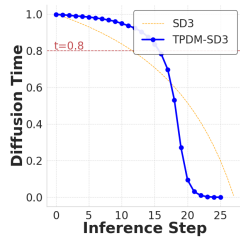
(c)



Prompt: An ornate, golden invitation letter with intricate calligraphy. The text reads 'Your Presence is Requested at the Royal Feast' in elegant, swirling script. The letter is illuminated by soft candlelight and rests on a royal velvet cushion. The background features a grand palace with towering spires and lush gardens, with a small scroll tucked inside the envelope.



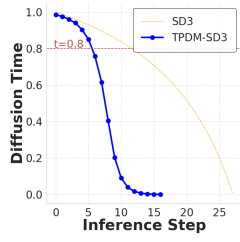
(e)



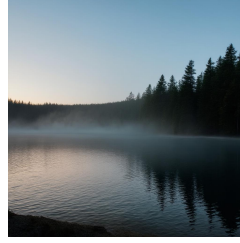
Prompt: Arctic ice, polar bears, drifting floes, aurora.



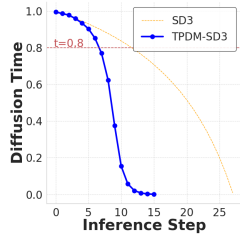
(b)



Prompt: Serenity over a lake, mist rising, dawn's first light, silent forest.



(d)



Prompt: An ancient, leather-bound book with embossed mystical symbols, open on a wooden desk in a dimly lit library. The pages are yellowed, filled with arcane illustrations and handwritten notes in an unknown script. A faint, ethereal glow emanates from the book, casting soft light on a quill and ink pot nearby. A crystal ball sits on the desk, reflecting the glow. Through an arched window, a full moon shines in a starry night sky, and a raven perches on the windowsill, its eyes fixed on the book. In the background, shelves are lined with other mysterious tomes, some with spines adorned with gems or strange markings.



(f)

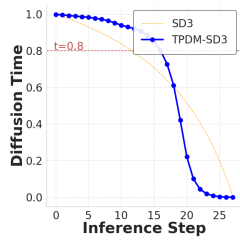


Figure 11. Prompts, images and predicted schedules.

D. Prompts to Generate Images in Fig. 1

1. 8k uhd A man looks up at the starry sky, lonely and ethereal, Minimalism, Chaotic composition Op Art.
2. A deep-sea exploration vessel descending into the pitch-black ocean, its powerful lights illuminating the glowing, alien creatures that inhabit the abyss. A massive, ancient sea creature with bioluminescent patterns drifts

into view, its eyes glowing as it watches the explorers from the shadows of an underwater cave.

3. Half human, half robot, repaired human.
4. A baby painter trying to draw very simple picture, white background.
5. an astronaut sitting in a diner, eating fries, cinematic, analog film.

6. Van Gogh painting of a teacup on the desk.
7. A galaxy scene with stars, planets, and nebula clouds.
8. A hidden, forgotten city deep in a jungle, with crumbling stone temples overgrown by thick vines. In the heart of the city, a mysterious glowing artifact lies on an ancient pedestal, surrounded by an eerie mist. Strange symbols shimmer faintly on the stone walls, waiting to be uncovered.
9. A lone astronaut stranded on a desolate planet, gazing up at the sky. The planet's surface is cracked and barren, with glowing, unearthly ruins scattered across the horizon. In the distance, a massive, alien ship slowly descends, casting an eerie shadow over the landscape.